Nano Energy 35 (2017) 138–145

Contents lists available at ScienceDirect

Nano Energy

journal homepage: www.elsevier.com/locate/nanoen

Full paper

One-pot synthesis of heterogeneous Co_3O_4-nanocube/$Co(OH)_2$-nanosheet hybrids for high-performance flexible asymmetric all-solid-state supercapacitors

Huan Pang[a], Xinran Li[a], Qunxing Zhao[b], Huaiguo Xue[a], Wen-Yong Lai[b,d], Zheng Hu[c], Wei Huang[b,d,*]

[a] School of Chemistry and Chemical Engineering, Yangzhou University, Yangzhou, Jiangsu 225002 China
[b] Key Laboratory for Organic Electronics and Information Displays (KLOEID) & Institute of Advanced Materials (IAM), Jiangsu National Synergetic Innovation Center for Advanced Materials (SICAM), Nanjing University of Posts & Telecommunications, 9 Wenyuan Road, Nanjing 210023, China
[c] Key Laboratory of Mesoscopic Chemistry of MOE, Jiangsu Provincial Lab for Nanotechnology, School of Chemistry and Chemical Engineering, Nanjing University, Nanjing 210093, China
[d] Key Laboratory for Organic Electronics and Information Displays (KLOEID) & Institute of Advanced Materials (IAM), Jiangsu National Synergetic Innovation Center for Advanced Materials (SICAM), Nanjing Tech University (NanjingTech), 30 South Puzhu Road, Nanjing 211816, China

ARTICLE INFO

Keywords:
Flexible supercapacitors
Energy storage
Hybrid electrodes
All-solid-state

ABSTRACTS

A novel heterogenous Co_3O_4-nanocube/$Co(OH)_2$-nanosheet hybrid is prepared by a controllable facile one-pot hydrothermal reaction. The resulting Co_3O_4 nanocubes are highly uniform in morphology, and are distributed uniformly on the individual $Co(OH)_2$ nanosheets. Such unique nanostructural features show significant advantages for applications as flexible supercapacitor electrodes in terms of enhanced durability and capacitance. The as-prepared electrode has offered a large capacitance of 1164 F g^{-1} at 1.2 A g^{-1}. When being paired with activated carbon, the resulting flexible all-solid-state device exhibited a maximum energy density of 9.4 mWh cm^{-3}. It is worthwhile noting that this as-assembled device showed little capacitance decay after over 5000 cycles with 97.4% retention of its original specific capacitance. Such a high performance outperforms most metal oxides-based electrodes and shows the advantages of the hybrid strategy, which shed light on exploring robust and cheap electrode materials for high-performance flexible supercapacitors.

1. Introduction

Electrochemistry provides us with solutions to the severe energy and environmental crisis facing humanity in the form of electrocatalysis and electrochemical energy storage. Both devices are calling for cheap electrode materials with decent performance. As one of the most promising energy storage devices, supercapacitors (SCs) have been intensively investigated in the past couple of years. How to design and synthesize novel electrode materials to achieve higher power/energy density in SCs is the key challenge to be overcome. There are mainly two kinds of electrode materials: carbon materials rely on charge accumulation at the surface to store charges, whereas metal oxides and conjugated polymers mainly rely on reversible redox reactions [1–3]. Accordingly, researchers define the capacitors based on carbon materials as electric-double-layer capacitors, and the capacitors based on reversible redox reactions as pseudocapacitors [4].

Many previous studies have confirmed that the charge storage capacity of SCs depends on both the natural characteristics of electrode materials and the special design of corresponding micro/nanostructure of the electrode materials. To improve the ion diffusion and electron transport efficiency at the electrode/electrolyte interface, extensive strategies have been proposed to design a functional heterostucture consisiting of the backbone support and active supercapacitive nanomaterials [5]. Different architectures, such as hybrid and core-shell structures, have been constructed. Of these architectures, hydroxides/oxides on graphene (carbon nanotubes) is an important and promising approach [6,7]. The graphene backbone can provide not only enhanced durability but also better electrical conductivity. The challenges are how to uniformly distribute the pseudocapacitive elements on the carbon backbone; how to control the size, phase, composition and morphology of pseudocapacitive elements; and how to develop general methods that apply to a wide range of pseudocapacitive materials [8].

* Corresponding author at: Key Laboratory for Organic Electronics and Information Displays (KLOEID) & Institute of Advanced Materials (IAM), Jiangsu National Synergetic Innovation Center for Advanced Materials (SICAM), Nanjing University of Posts & Telecommunications, 9 Wenyuan Road, Nanjing 210023, China.
E-mail addresses: iamwylai@njupt.edu.cn (W.-Y. Lai), zhenghu@nju.edu.cn (Z. Hu), wei-huang@njtech.edu.cn (W. Huang).

http://dx.doi.org/10.1016/j.nanoen.2017.02.044
Received 22 December 2016; Received in revised form 15 February 2017; Accepted 22 February 2017
Available online 10 March 2017

The hydroxides/oxides on graphene (carbon nanotubes) hybrid structure can be extended. For instance, pseudocapacitive materials, like MnO_2 [9,10], $Ni(OH)_2$ [11], Nickel [12], FeO_x [13], and others [14–17], are anchored to other pseudocapacitive platforms such as metal oxides/hydroxides, and conductive polymers in various types to form heterogeneous nanostructures. For example, Mai et al. successfully fabricated hierarchical core-shell $MnMoO_4/CoMoO_4$ heterogeneous nanowires as high-performance supercapacitive materials by a mild method, which offered a specific capacitance of 187.0 F g^{-1} at a current density of 1 A g^{-1} [18]. Hu et al. demonstrated a novel mesostructured NiO/Ni composite, which was made of NiO/Ni heterostructure at the mesoscale, which achieved an ultrahigh specific capacity of up to 522 C g^{-1} at current density of 1 A g^{-1} [19]. Wu et al. reported a novel supercapacitor electrode composed of multicomponent $MnCo_2O_4$@ $Ni(OH)_2$ belt-based core-shell nanoflowers in a facile and cost-effective way, which exhibited a significantly enhanced specific capacitance [20]. However, synthesis of these composites generally involves lengthy procedures with at least two or more steps, which makes the synthesis time-consuming and thus limits their practical applications. Furthermore, the size, phase, composition and morphology of the dotting elements are far from controllable. Lastly, due to the presence of defects, it is difficult to achieve uniform distribution of the dotting elements. Thus, it is highly desirable to develop more efficient methodology to simplify the preparation procedures.

Cobalt oxides and hydroxides have a very large theoretical pseudocapacitance of 3500–4600 F g^{-1} with a potential window of 0.45 V [21]. A large number of micro/nanostructured cobalt oxide/hydroxide materials have been synthesized by different methods, and corresponding electrochemical capacitor behaviors have been investigated in the past few years [21–24]. However, highly conductive cobalt oxides always show small surface area, while cobalt hydroxides with high surface area have low conductivity. Such drawback has greatly limited the rapid development and practical application of cobalt oxides/hydroxides as electrode materials. In this work, a controllable facile one-pot hydrothermal methodology has been developed and heterogenous Co_3O_4-nanocube/$Co(OH)_2$-nanosheet hybrids (Denoted as "$Co_3O_4/Co(OH)_2$ hybrids") with well-defined nanostructured morphology have been successfully synthesized in one step. The controllable uniform growth and distribution of Co_3O_4 nanocubes on the $Co(OH)_2$ nanosheets results in unique well-defined surface-interface nanostructures. In addition, the Co_3O_4 nanocubes are highly uniform in morphology, and are distributed uniformly on the $Co(OH)_2$ nanosheets. Electrochemical measurements showed that the $Co_3O_4/Co(OH)_2$ hybrid electrode exhibited a large specific capacitance (1164 F g^{-1}). Besides, the as-prepared $Co_3O_4/Co(OH)_2$ hybrids with activated carbon (AC) were paired to build a flexible asymmetric all-solid-state supercapacitor (ASC). Inspiringly, the maximum energy density is up to 9.4 mWh cm^{-3} with excellent cycle stability even after 5000 cycles, which outperforms most metal oxides-based electrochemical energy storage devices ever reported.

2. Experimental section

2.1. Material preparation

2.1.1. Typical synthesis of heterogeneous $Co_3O_4/Co(OH)_2$ hybrids

For 0.291 g, $Co(NO_3)_2{\cdot}6H_2O$ (1 mmol) was dissolved in 20 mL 0.1 M NaOH solution. The above solution was transferred into 100 mL autoclave with a Teflon liner at 100 °C, and kept for 12 h. The obtained product was filtered, and then washed with H_2O and ethanol for several times. At last, the sample was dried naturally in air.

2.1.2. Typical synthesis of Co_3O_4 nanocubes

0.291 g, $Co(NO_3)_2$ $6H_2O$ (1 mmol) was dissolved in 20 mL 0.1 M NaOH solution. The obtained solution was transferred into 100 mL autoclave with a Teflon liner at 200 °C, and kept for 24 h. The obtained product was filtered, and then washed with H_2O and ethanol for several times, and dried naturally in air.

2.1.3. Typical synthesis of Co_3O_4 microplates

0.291 g, $Co(NO_3)_2$ $6H_2O$ (1 mmol) was dissolved in 20 mL H_2O. Meanwhile 2 mL octadecenylamine and 10 mL ethanol were mixed together to form a homogeneous mixture, which was added into the above $Co(NO_3)_2$ solution under stirring for 30 min to form a green mixture. The obtained mixture was transferred into 40 mL autoclave with a Teflon liner, and kept at 180 °C for 12 h. The resulting product was filtered, and then washed by H_2O and ethanol for several times, and dried in the air naturally.

2.1.4. Typical synthesis of Co_3O_4+$Co(OH)_2$ hybrids

0.020 g Co_3O_4 nanocubes and 0.180 g $Co(OH)_2$ microplates were dispersed into 20 mL ethanol, and then was stirred for 60 min to form a black mixture. The obtained mixture was filtered, and dried in air naturally.

2.2. Characterizations

The products were tested by X-ray diffraction (XRD) on a Rigaku-Ultima III with Cu K_α radiation (λ=1.5418 Å) for the phase analyses. Field-emission scanning electron microscope (FE-SEM, JEOL JSM-6701F) and transmission electron microscopy (TEM, JEM-2100) were used for observing the morphology of the samples at an acceleration voltage at 5.0 kV and 200 kV, respectively. Nitrogen adsorption-desorption properties of the samples were measured on the Gemini VII 2390 Analyzer using the volumetric method at 77 K. The specific surface area was obtained by the Brunauer-Emmett-Teller (BET) method from the N_2 adsorption-desorption isotherms. Atomic force microscope (AFM, Benyuan-CSPM4000) images were also measured.

2.3. Electrochemical measurements

2.3.1. Fabrication of working electrodes

Activated materials (The heterogeneous $Co_3O_4/Co(OH)_2$ hybrids, Co_3O_4 nanocubes, $Co(OH)_2$ microplates or Co_3O_4+$Co(OH)_2$ hybrids), acetylene black, and polytetrafluoroethylene (PTFE) were well mixed to form a mixture with a weight ratio of 80:15:5. Then we coated such mixture on the nickel foam (The area=1×1 cm^2), and pressed the nickel foam to a thin foil with a pressure of 5.0 MPa. It is about 5 mg for the weight of activated materials.

2.3.2. Electrochemical characterization on working electrodes

Electrochemical measurements were carried out on an electrochemical working station (CHI 660D, Shanghai Chenhua) in a three-electrode system. The platinum electrode was as a counter electrode, and the Hg/HgO electrode was the reference electrode in the three-electrode system. We firstly blew Ar gas into the solution for removing O_2 gas before electrochemical testing. The electrolyte solution was 3.0 M KOH solution. Cyclic voltammetry and galvanostatic charge-discharge methods were applied for confirming the capacitive behavior of working electrodes.

2.3.3. Assembling of flexible ASC devices

Firstly, the polyethylene terephthalate (PET) film was plated with a Pt layer with the thickness of 3–5 nm, and then the activated materials were coated on the PET film. The activated materials (containing positive electrode materials: $Co_3O_4/Co(OH)_2$ hybrids-3.1 mg, Co_3O_4 nanocubes-2.8 mg, $Co(OH)_2$ microplates-2.6 mg or Co_3O_4+$Co(OH)_2$ hybrids-2.9 mg; and negative electrode material: activated carbon) were mixed in the same way as that in the three electrode system, which were applied as the working electrode after naturally drying. The weight ratio of the negative electrode to the positive electrode is 1:6.5. The gel electrolyte was obtained as follows: 1.52 g poly(vinylalcohol)

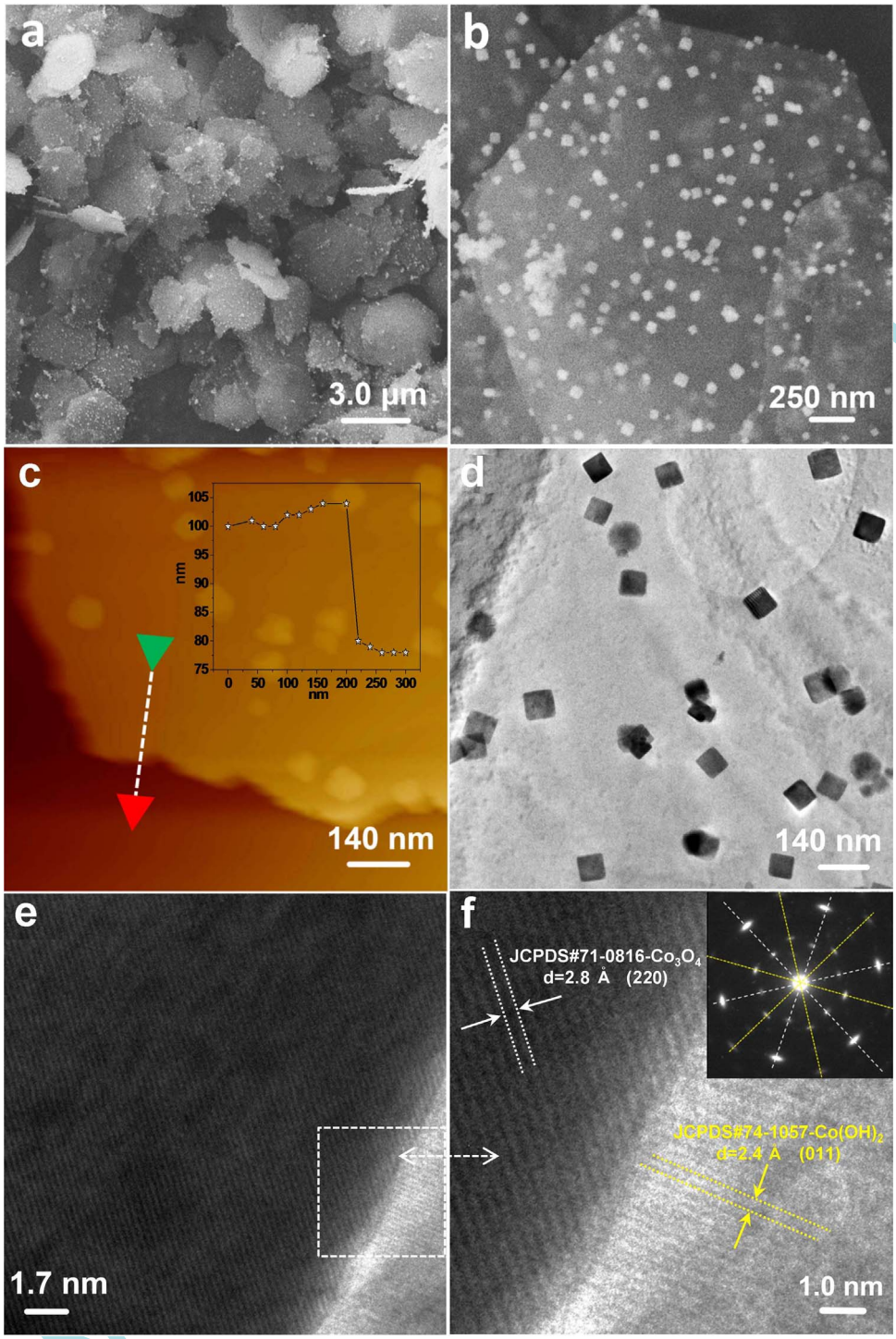

Fig. 1. a,b) SEM images of as-prepared $Co_3O_4/Co(OH)_2$ hybrids, c) AFM image, Inset-corresponding height section image, d) TEM image, and e,f) HRTEM images, Inset-SAED patterns.

(PVA), 2.13 g KOH, and 15 mL H_2O were well mixed at 75 °C for 30 min, and dropped onto the obtained cool gel to cover the activated material. After 5–10 min, a layer of solid electrolyte was formed, and then two pieces of as-prepared electrodes with solid electrolyte were pressed together. Namely, the flexible ASC device was successfully fabricated.

3. Results and discussion

The phase and crystal structure of the as-prepared products were analyzed by X-ray diffraction (XRD) patterns (Fig. S1a). The typical diffraction peaks in XRD patterns are in good accordance with Co_3O_4 (JCPDS cards No.71-0816) and $Co(OH)_2$ (JCPDS cards No.74-1057). However, there are only two weak peaks (Marked by "*") of Co_3O_4, which indicates that only a tiny amount of the Co_3O_4 has been formed. On the contrary, most of the strong peaks are indexed to $Co(OH)_2$. More importantly, $Co_3O_4/Co(OH)_2$ hybrids have been successfully prepared by a facile and simple one-pot hydrothermal methodology without any surfactants (Detailed information is shown in the experimental section).

As shown in Fig. 1, the morphology of as-prepared samples was measured by field emission scanning electron microscopy (FESEM),

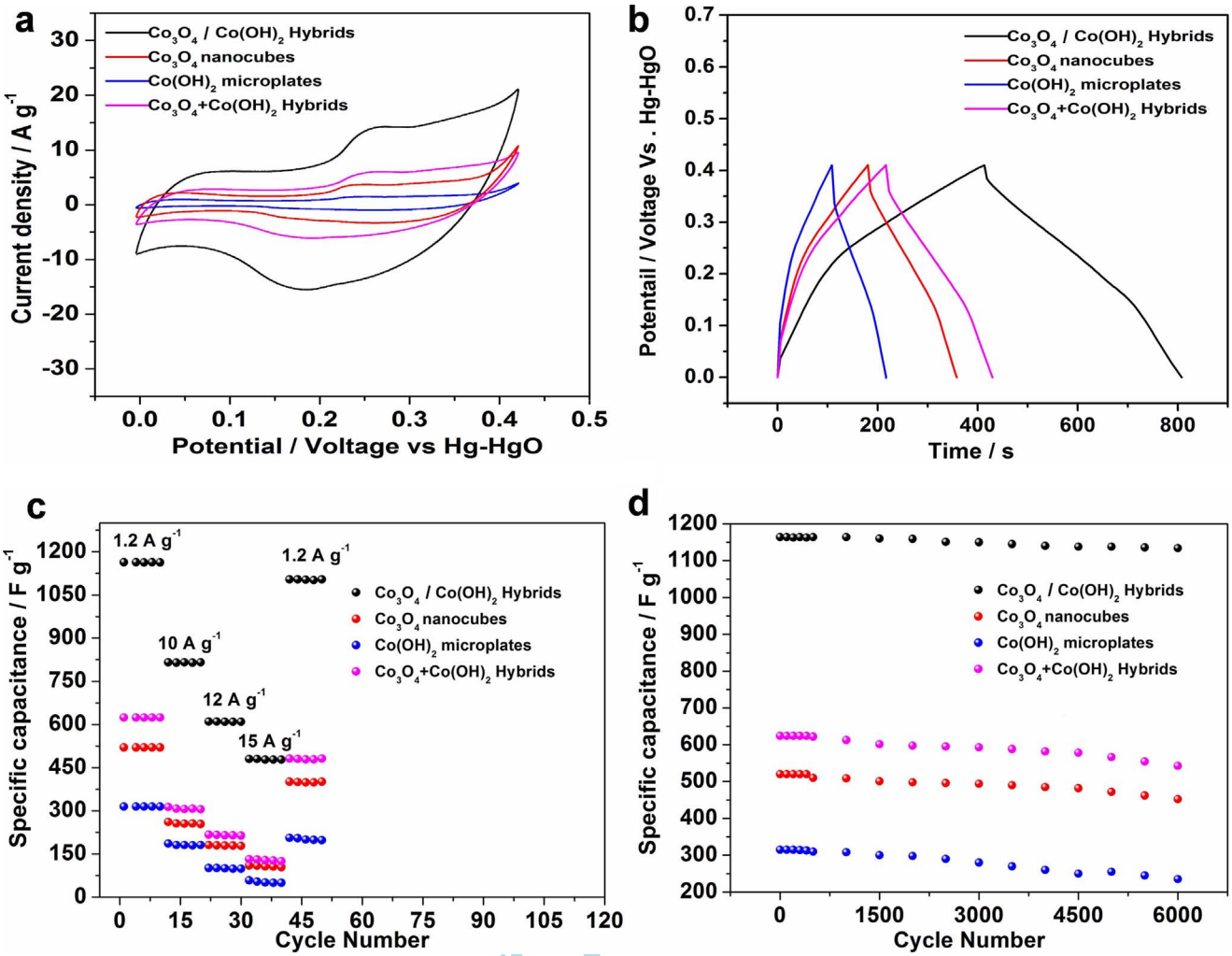

Fig. 2. Electrochemical results of as-prepared electrodes (The $Co_3O_4/Co(OH)_2$ hybrids, Co_3O_4 nanocubes, $Co(OH)_2$ microplates and Co_3O_4+$Co(OH)_2$ hybrids), a) CV curves with a scan rate at 10 mV s^{-1}; b) Galvanostatic charge-discharge curves at a current density 1.2 A g^{-1}, 0.0–0.41 V; c) The specific capacitance changing *vs.* different current densities from 1.2 A g^{-1} to 15 A g^{-1}, and d) Cycling performance at 1.2 A g^{-1} for 6000 cycles.

atomic force microscopy (AFM), and transmission electron microscopy (TEM). From Fig. 1a, it is seen that the $Co_3O_4/Co(OH)_2$ hybrids have been obtained, and the size of a single hybrid is about 2.5–3.0 μm. Clearly, there are many Co_3O_4 nanocubes distributed on the $Co(OH)_2$ nanosheets as shown in Fig. 1b and these Co_3O_4 nanocubes show the size of 60 nm. Interestingly, the thickness of the $Co(OH)_2$ nanosheet can also be determined by AFM. According to the analysis of the height profile in Fig. 1c, the thickness of the $Co(OH)_2$ nanosheet is observed to be 22 nm. To evaluate the thickness of $Co(OH)_2$ nanosheet directly, high magnification SEM images from the lateral view of the nanosheet have been recorded as supplied in Fig. S2. It is estimated that the thickness of $Co(OH)_2$ nanosheet is also about 20 nm from the SEM images. Furthermore, the hybrid structure is further confirmed by TEM as shown in Fig. 1d-f. Co_3O_4 nanocubes are uniformly distributed on the $Co(OH)_2$ nanosheet with nearly no aggregations as shown in Fig. 1d. The HRTEM images of the surface-interfaces of the Co_3O_4/$Co(OH)_2$ hybrid are shown in Fig. 1e and f. The measured distance of neighboring lattice fringes in the left of Fig. 1f is 0.28 nm, corresponding well to the (220) lattice spacing of Co_3O_4. Furthermore, the other neighboring lattice fringe distance in the right of Fig. 1f is 0.24 nm, according well with the (011) lattice spacing of $Co(OH)_2$. Moreover, the good crystalline characteristics of Co_3O_4 and $Co(OH)_2$ are further confirmed by the selected area electron diffraction (SAED) pattern as shown in the up-right-inset of Fig. 1f. Because $Co(OH)_2$ is very sensitive to the reaction temperature, $Co(OH)_2$ nanosheets are easily, instantaneously transformed into CoO_x with increasing the temperature or prolonging the reaction time. In our trials, we found that it was difficult to adjust the size or content of Co_3O_4 nanocubes *via* changing the hydrothermal conditions for the resulting hybrids.

For the comparison, we have synthesized Co_3O_4 nanocubes and $Co(OH)_2$ microplates (Detailed information seen in experimental section) respectively. Intererestingly, we have also mechanical mixed Co_3O_4 nanocubes and $Co(OH)_2$ microplates together with the mass ratio of 10:90, and the obtained mixture is named by "Co_3O_4+$Co(OH)_2$ hybrids". The corresponding SEM images and XRD patterns are shown in Figs. S3 and S4. The typical diffraction peaks in the XRD patterns are also in good accordance with Co_3O_4-JCPDS cards: no. 71-0816 in Fig. S3a, and $Co(OH)_2$-JCPDS cards: no. 74-1057 in Fig. S3b. The XRD patterns of Co_3O_4+$Co(OH)_2$ hybrids are indexed to two phases of $Co(OH)_2$ and Co_3O_4 in Fig. S3c. Interestingly, the size of Co_3O_4 nanocubes is about 60 nm in Fig. S4a,b, and that of $Co(OH)_2$ microplates is about 3.0 μm in Fig. S4c,d, whose sizes are according with those of the $Co_3O_4/Co(OH)_2$ hybrid structure. It is reasonable for the comparison in the same micro/nanoscale. However, some Co_3O_4 nanocubes have got together in Fig. S4e, while some $Co(OH)_2$ microplates without any Co_3O_4 nanocubes due to the mechanical mixing in Fig. S4f.

Brunauer-Emmett-Teller (BET) measurements have been used to obtain the pore size distribution and porous information of the samples. The as-prepared $Co_3O_4/Co(OH)_2$ hybrids, $Co(OH)_2$ micro-

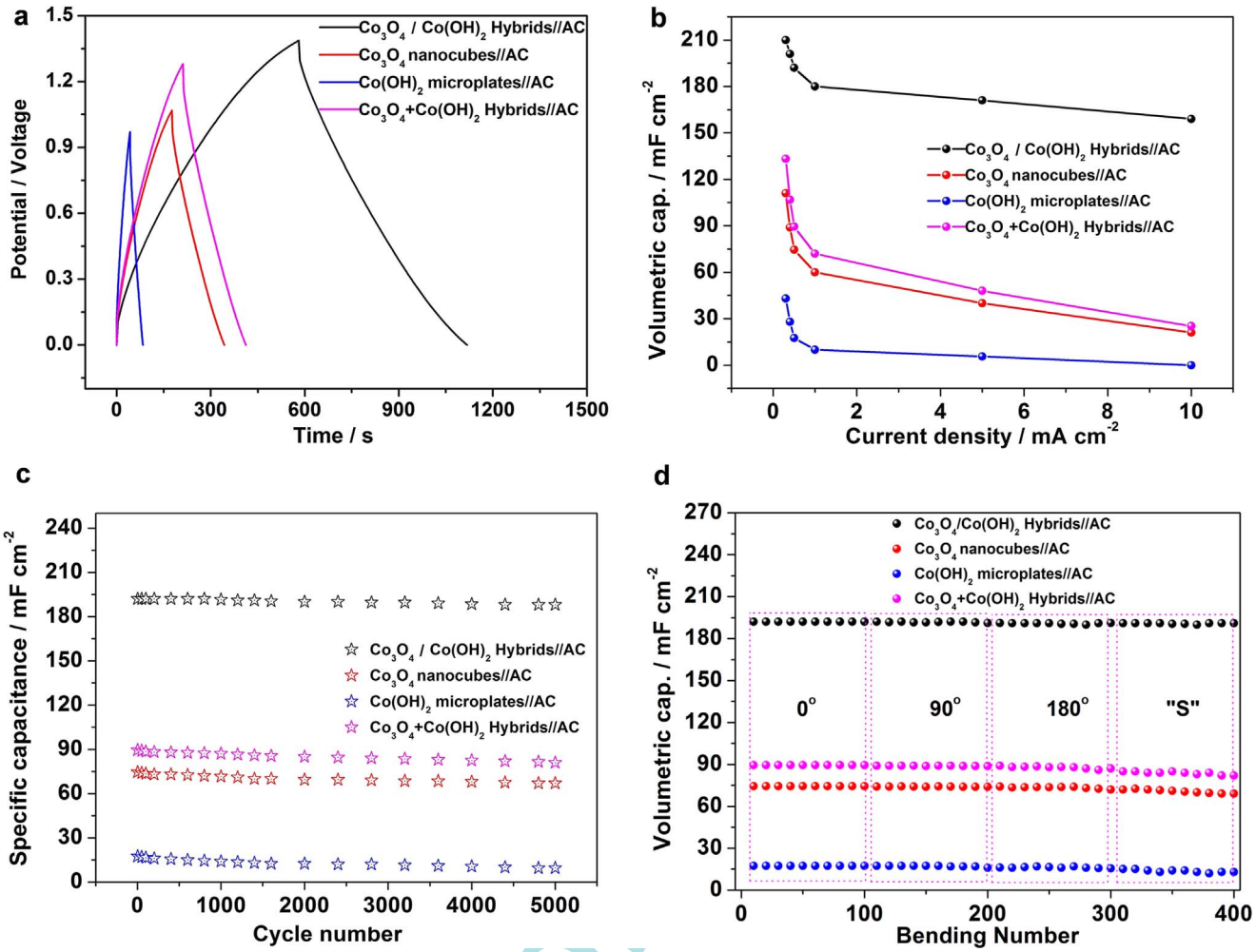

Fig. 3. Electrochemical results of as-prepared flexible ASC devices (Co_3O_4/$Co(OH)_2$ hybrids//activated carbons, Co_3O_4 nanocubes//activated carbons, and $Co(OH)_2$ microplates//activated carbons, and Co_3O_4+$Co(OH)_2$ hybrids//activated carbons): a) Charge-discharge curves at 0.5 mA cm^{-2} of as-prepared devices in different potential windows, b) The specific capacitance was calculated based on the data in a, c) Cycling performance at 0.5 mA cm^{-2} for 5000 cycles, and d) As-prepared ASC devices under different bending degrees (0°, 90°, 180° and "S"), and each bending degree with 100 cycles.

plates, and Co_3O_4+$Co(OH)_2$ hybrids present a distinct hysteresis in the range of 0.75–1.0 P/P0 as shown in Fig. S5a, indicating that the presence of pores is possibly formed by the stacking of component nanoparticles. The BET surface area of Co_3O_4/$Co(OH)_2$ hybrids (56.8 m^2 g^{-1}) is close to that of $Co(OH)_2$ microplates (69.3 m^2 g^{-1}) and Co_3O_4+$Co(OH)_2$ hybrids (59.3 m^2 g^{-1}), but it is larger than that of Co_3O_4 nanocubes (22.9 m^2 g^{-1}). The corresponding curves of Barrett-Joyner-Halenda (BJH) pore size distribution (Fig. S5b) suggest that the average pore size of Co_3O_4/$Co(OH)_2$ hybrids is about 15 nm, while few pores are observed in other three samples. Generally speaking, a large number of mesopores always play a critical role in electrochemical processes, which can effectively facilitate guest ion/molecule transport and electrolyte penetration, contributing to an ultra-high electrochemical performance.

To confirm the formation of the Co_3O_4/$Co(OH)_2$ hybrids, X-ray photoelectron spectroscopy (XPS) analysis of Co_3O_4/$Co(OH)_2$ hybrids, Co_3O_4 nanocubes, $Co(OH)_2$ microplates, and Co_3O_4+$Co(OH)_2$ hybrids was conducted (Fig. S6a). The peak at around 781.2 eV is attributed to Co 2p3/2 for $Co(OH)_2$ microplates, indicating the only valence state of Co is Co(II). What is more, the peaks of Co_3O_4/$Co(OH)_2$ hybrids, Co_3O_4 nanocubes, and Co_3O_4+$Co(OH)_2$ hybrids are also observed at around 780.1 eV, which means that Co(II) and Co(III) co-exist in this system. In the Co 2p spectra as shown in Fig. S6b,c, two major peaks were recorded with a spin-energy separation of 16.1 eV for Co_3O_4/$Co(OH)_2$ hybrids and 15.7 eV for Co_3O_4+$Co(OH)_2$ hybrids, which suggests that the density of the electron cloud around Co is different. What's more, this different electron cloud density is likely to affect the electron transfer in the electrochemical process. The XPS analysis has indirectly confirmed the formation of the Co_3O_4/$Co(OH)_2$ hybrid, and the hybrid shows synergistic effect between the respective features of the constituents.

In a three-electrode system, cyclic voltammogram (CV) curves of the as-prepared Co_3O_4/$Co(OH)_2$ hybrid, Co_3O_4 nanocube, $Co(OH)_2$ microplate, and Co_3O_4+$Co(OH)_2$ hybrid electrodes at a scan rate of 10 mV s^{-1} in the potential range of 0–0.41 V (*vs.* Hg-HgO) were obtained as shown in Fig. 2a. The electrolyte was 3.0 M KOH solution. From the shapes of these curves, the as-prepared electrodes mainly offer pseudocapacitive behavior which differs from the electric double-layer behavior. Obviously, the surrounding area from the CV curve of Co_3O_4/$Co(OH)_2$ hybrid electrode is larger than that of Co_3O_4 nanocube electrode, $Co(OH)_2$ microplate electrode, and Co_3O_4+$Co(OH)_2$ hybrid electrode. The charge-discharge curves of the as-prepared electrodes are measured at 1.2 A g^{-1}. It was also found the charge-discharge curve of the Co_3O_4/$Co(OH)_2$ hybrid electrode shows the longest charge-discharge time as shown in Fig. 2b. By means of changing the current density from 1.2 to 15.0 A g^{-1}, the corresponding specific capacitance was still 478 F g^{-1} at 15.0 A g^{-1} as shown in Fig. 2c (The calculation is shown in the calculation section of the Supporting Information). The corresponding specific capacitance was as high as 1104 F g^{-1} when recovering to 1.2 A g^{-1}, demonstrating the outstanding rate capability

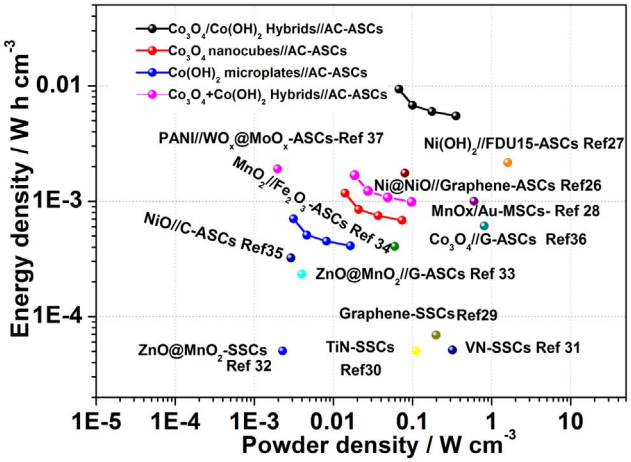

Fig. 4. Power density and energy density of the as-prepared ASC devices.

of the $Co_3O_4/Co(OH)_2$ hybrid electrode. Furthermore, the cycle life stability of as-prepared electrodes has also been investigated as shown in Fig. 2d. After 6000 cycles at 1.2 A g^{-1}, the $Co_3O_4/Co(OH)_2$ hybrid electrode shows a long-term cycle ability and the corresponding specific capacitance is 1134 F g^{-1}, offering only 2.6% decay compared with its initial performance. On the contrary, large decay were found for Co_3O_4 nanocube electrode (13.1%), $Co(OH)_2$ microplate electrode (25.4%), and Co_3O_4+$Co(OH)_2$ hybrid electrode (14.1%) as depicted in Fig. 2d. The stable specific capacitance can be attributed to the specific nanostructure of the $Co_3O_4/Co(OH)_2$ hybrids, providing effective ion diffusion and charge transfer on the resulting unique surface-interface structures.

The activated carbon was purchased from Fuzhou Yihuan carbon company (Fuzhou, China), and the morphology of the activated carbon is shown in Fig. S7. It is seen the activated carbon materials are amorphous particles in ten micrometers. The galvanostatic charge-discharge curves of the activated carbon electrode and corresponding specific capacitances are shown in Fig. S8. The specific capacitance of purchased activated carbon electrode was 262 F g^{-1} when the current density was 1.2 A g^{-1}. Thus, the mass ratio between the positive and negative electrode was set at 1:6.5 in the as-assembled device.

Flexible ASC devices were fabricated based on the as-prepared product and activated carbon as electrode materials ($Co_3O_4/Co(OH)_2$ hybrids// activated carbons, Co_3O_4 nanocubes//activated carbons, $Co(OH)_2$ microplates//activated carbons, and Co_3O_4+$Co(OH)_2$ hybrids//activated carbons) according to our previously reported method [25] (See more details in experimental section, and a simple structure of as-prepared flexible ASC devices is shown in Fig. S9). Fig. S10 shows CV curves of the as-prepared flexible ASC devices at different voltages ranging from 0.0 to 0.97 V to 0.0–1.40 V with the scan rate of 10 mV s^{-1}. When increasing the operating potential to 1.40 V, the largest surrounding area is from the CV curve of $Co_3O_4/Co(OH)_2$ hybrids//activated carbons, and it elucidates the potential at which most Faradic reactions has occurred.

As shown in Fig. 3a, galvanostatic charge-discharge curves of the flexible ASC devices at 0.5 mA cm^{-2} suggest that the $Co_3O_4/Co(OH)_2$ hybrids//activated carbons have the highest charge-discharge potential (1.40 V), which are higher than that of Co_3O_4 nanocubes//activated carbons (1.07 V), $Co(OH)_2$ microplates//activated carbons (0.97 V) and Co_3O_4+$Co(OH)_2$ hybrids//activated carbons (1.28 V). According to the equation $E=0.5\,C\times V^2$ (Where E is the stored energy, C is the specific capacitance and V is the operating voltage. Detailed information is shown in calculation section in Supporting Information), the amount of the stored energy of the flexible ASC device (The operating voltage is 0–1.40 V) can be enhanced by at least 2.08-fold compared with those of $Co(OH)_2$ microplates//activated carbons with the operating voltage of 0–0.97 V. Subsequently, specific capacitances of as-prepared devices with different current densities are shown in Fig. 3b (The calculation is shown in calculation section in Supporting Information). The specific capacitance of the $Co_3O_4/Co(OH)_2$ hybrids//activated carbons can reach 210 mF cm^{-2} when the current density is 0.3 mA cm^{-2}, much better than that of Co_3O_4 nanocubes// activated carbons (111 mF cm^{-2}), $Co(OH)_2$ microplates//activated carbons (43 mF cm^{-2}) and Co_3O_4+$Co(OH)_2$ hybrids//activated carbons (133 mF cm^{-2}). Interestingly, at the current density of 10 mA cm^{-2}, the flexible $Co_3O_4/Co(OH)_2$ hybrids//activated carbons ASC device offers good rate capability by maintaining the capacitance of 159 mF cm^{-2}.

Cycling life of the ASC device is crucial in practical application. Therefore, cycling tests of as-prepared ASC devices after 5000 cycles are performed as shown in Fig. 3c. Obviously, the capacitance of the Co_3O_4 nanocubes//activated carbons device and $Co(OH)_2$ microplates//activated carbons devices decreased after 5000 cycles, while the $Co_3O_4/Co(OH)_2$ hybrids//activated carbons device showed little decay (2.4%). Coulombic efficiency of as-prepared flexible ASC devices is shown in Fig. S11. The flexible $Co_3O_4/Co(OH)_2$ hybrids//activated carbons ASC device offers a good coulombic efficiency (94%) even after 5000 cycles. To measure the flexibility of the as-prepared ASC devices, the as-prepared ASC devices were tested under different bending degrees (0°, 90°, 180° and "S") for each 100 cycles. It is clear that as-prepared ASC devices showed good flexibility, enabling the as-prepared ASC devices to work well under flexible conditions.

Power density and energy density of the as-prepared ASC devices are depicted in Fig. 4, in comparison with recent results of supercapacitor devices [26–37]. The $Co_3O_4/Co(OH)_2$ hybrids//activated carbons device exhibited a peak volumetric energy density of 9.4 mW h cm^{-3}. Additionally, the peak power density of the flexible ASC device was 354 mW cm^{-3} at 10.0 mA cm^{-2}. The maximum energy density of $Co_3O_4/Co(OH)_2$ hybrids//activated carbons device was larger than those shown in Fig. 4. Furthermore, the as-prepared flexible $Co_3O_4/Co(OH)_2$ hybrids//activated carbons device in this work outperforms most recent results in terms of the maximum power density including Ni@NiO//Graphene [26], Graphene// Graphene [29], TiN//TiN [30], VN//VN [31], ZnO@MnO_2//ZnO@MnO_2 [32], ZnO@MnO_2// Graphene [33], MnO_2//Fe_2O_3 [34], NiO//C [35], and PANI//WO_x@MoO_x [37], while it is lower than those of some other devices, such as ($Ni(OH)_2$//FDU15 [27], MnO_x/Au [28], and Co_3O_4// Graphene [36]) as shown in Fig. 4. More importantly, the weight of Co_3O_4@$Co(OH)_2$ hybrids//activated carbons device is so light that it can be held by the dandelion flower as shown in Fig. S12. A red light-emitting diode (LED) can be powered for 5 min after the $Co_3O_4/Co(OH)_2$ hybrids// activated carbons device was only charged for 30 s as illustrated by Fig. S13.

The $Co_3O_4/Co(OH)_2$ hybrids//activated carbons device was further assembled either in series or in parallel to meet specific energy needs for different applications. Charge-discharge curves of a single device and four flexible ASC devices ($Co_3O_4/Co(OH)_2$ hybrids//activated carbons in series at 0.5 mA cm^{-2} are plotted in Fig. S14. Interestingly, the charge-discharge voltage window for the four devices connected in series is approximate four times that of a single device. What's more, The charge-discharge time is four times as long as that for a single device as illustrated in Fig. S15 that shows the galvanostatic charge-discharge curves for a single device and four flexible ASC devices ($Co_3O_4/Co(OH)_2$ hybrids//activated carbons) in parallel at 2.0 mA cm^{-2}.

It is obvious that the as-prepared $Co_3O_4/Co(OH)_2$ hybrid demonstrated good energy-density as an electrode material for flexible ASCs. The electrochemical impedance spectrum of as-prepared devices were in the frequency of 0.01–10^5 Hz under the open-circuit circumstances at room temperature, as shown in Fig. S16. The high region part of EIS (100000–100 Hz) is shown in Fig. S16a and the equivalent circuit for the electrochemical impedance spectrum is shown in the inset of Fig. S16a. Besides, the charge-transfer resistance (R_{ct}) of this device was calculated by the ZsimpWin software. The $Co_3O_4/Co(OH)_2$ hybrids//

activated carbons exhibited a low value of R_{ct}-75 Ω similar to that of Co_3O_4 nanocubes//activated carbons device (R_{ct}-71 Ω), $Co(OH)_2$ microplates//activated carbons device (R_{ct}-105 Ω) and Co_3O_4+$Co(OH)_2$ hybrids//activated carbons device (R_{ct}-83 Ω). The probable reasons are as follows: 1) Due to the coexistence of Co_3O_4 nanocubes, the Co_3O_4/$Co(OH)_2$ hybrids//activated carbon device has smaller charge-transfer resistance than the single $Co(OH)_2$ microplates//activated carbon device. 2) The Co_3O_4/$Co(OH)_2$ hybrids can offer larger specific capacitance than that of Co_3O_4 at the same weight. The possible charge-discharge mechanism for Co_3O_4 and $Co(OH)_2$ is as following:

$$Co_3O_4+OH^-=H_2O+3CoOOH+e^- \quad (1)$$

$$Co(OH)_2+OH^-=CoOOH+H_2O+e^- \quad (2)$$

$$CoOOH+OH^-=CoO_2+H_2O+e^- \quad (3)$$

$$Co_3O_4+4OH^-=3CoO_2+2H_2O+4e^- \quad (4)$$

$$Co(OH)_2+2OH^-=CoO_2+2H_2O+2e^- \quad (5)$$

Eqs. (4) and (5) are full electrochemical charge-discharge mechanism equations of Co_3O_4 and $Co(OH)_2$, respectively. When the potential window is 0.45 V, the maximum theoretical capacitance of $Co(OH)_2$ is 4613 F g^{-1}, which is much better than that of the maximum theoretical capacitance of Co_3O_4 (3561 F g^{-1}). Clearly, when the weight of the activated materials is the same, $Co(OH)_2$ can offer larger specific capacitance than that of Co_3O_4. Interestingly, although both Co_3O_4 nanocubes and $Co(OH)_2$ microplates were noticed for the Co_3O_4+$Co(OH)_2$ hybrid, the conductivity of the Co_3O_4+$Co(OH)_2$ hybrid electrode has not been much improved as depicted in Fig. S16. The hybrid obtained from the mechanical mixing is not stable which also offers a low coulombic efficiency as shown in Fig. S11. In contrast, the Co_3O_4/$Co(OH)_2$ hybrid structure can largely increase the electrode conductive ability and its electrochemical capacitance.

4. Conclusions

In summary, a heterogeneous Co_3O_4/$Co(OH)_2$ hybrid was successfully prepared by a controllable facile one-pot hydrothermal reaction. The results show that the Co_3O_4 nanocubes are highly uniform in morphology, and are distributed uniformly on the individual $Co(OH)_2$ nanosheets. Such unique nanostructural features show significant advantages for applications as flexible supercapacitor electrodes in terms of enhanced durability and capacitance. The as-prepared electrode has offered a large capacitance of 1164 F g^{-1} at 1.2 A g^{-1}. When being paired with activated carbon, the resulting flexible all-solid-state device exhibited a maximum energy density of 9.4 mWh cm^{-3}, manifesting superior performance over those of Co_3O_4 nanocubes//activated carbon ASC device and $Co(OH)_2$ microplates//activated carbon ASC device, which resulted from the novel surface-interface structure of the Co_3O_4/$Co(OH)_2$ hybrid. It is worthwhile to mention that this as-assembled device offered little capacitance decay after over 5000 cycles. The retention of specific capacitance was 97.4%. In addition, the Co_3O_4/$Co(OH)_2$ hybrids//activated carbon ASC device showed excellent bending stability from 0° to 180°. Owing to the benefits of a simple synthetic process, facile fabrication and excellent performance, the Co_3O_4/$Co(OH)_2$ hybrids//activated carbon ASC device shows promising features for flexible, portable and lightweight electronic applications. By virtue of the versatility of metal oxide and hydroxide, the synthesis methodology presented here can be extended to the preparation of other metal oxide and hydroxide derived functional materials toward energy storage and conversion.

Acknowledgements

We acknowledge financial support from the National Key Basic Research Program of China (973 Program, 2014CB648300), the Program for New Century Excellent Talents in University (grant no. NCET-13-0645, and NCET-13-0872), the National Natural Science Foundation of China (21671170, 21422402, 21674050, 61136003 and 61106036), the Program for Innovative Research Team (in Science and Technology) in University of Henan Province (14IRTSTHN004), the Natural Science Foundation of Jiangsu Province (BK20140060, BK20130037, BM2012010), Specialized Research Fund for the Doctoral Program of Higher Education (20133223110008), the Ministry of Education of China (IRT1148), the Program for Graduate Students Research and Innovation of Jiangsu Province (CXZZ12-0454), the Synergetic Innovation Center for Organic Electronics and Information Displays, the Priority Academic Program Development of Jiangsu Higher Education Institutions (PAPD), the Six Talent Plan (2012XCL035, and 2015XCL030) and Qing Lan Project of Jiangsu Province.

Appendix A. Supporting information

Supplementary data associated with this article can be found in the online version at doi:10.1016/j.nanoen.2017.02.044.

References

[1] Y.G. Wang, H.Q. Li, Y.Y. Xia, Adv. Mater. 18 (2006) 2619.
[2] J. Yan, Q. Wang, T. Wei, Z. Fan, Adv. Energy Mater. 4 (2014) 1300816.
[3] D. Tai Dam, J.M. Lee, Nano Energy 2 (2013) 1186.
[4] H. Chen, L. Hu, M. Chen, Y. Yan, L. Wu, Adv. Funct. Mater. 24 (2014) 934.
[5] C. Yuan, L. Yang, L. Hou, L. Shen, X. Zhang, X. Lou, Energy Environ. Sci. 5 (2012) 7883.
[6] H. Wang, J.T. Robinson, G. Diankov, H.J. Dai, J. Am. Chem. Soc. 132 (2010) 3270.
[7] D.Y. Wang, M. Gong, H.L. Chou, C.J. Pan, H.A. Chen, Y.P. Wu, M.C. Lin, M.Y. Guan, J. Yang, C.W. Chen, Y.L. Wang, B.J. Hwang, C.C. Chen, H.J. Dai, J. Am. Chem. Soc. 137 (2015) 1587.
[8] Y.Y. Liang, Y.G. Li, H.L. Wang, H.J. Dai, J. Am. Chem. Soc. 135 (2013) 2013.
[9] C. Yuan, L. Yang, L. Hou, L. Shen, X. Zhang, X. Lou, Energy Environ. Sci. 5 (2012) 7883.
[10] J. Zhi, W. Zhao, X.Y. Liu, A.R. Chen, Z.Q. Liu, F.Q. Huang, Adv. Funct. Mater. 24 (2014) 2013.
[11] G.P. Wang, L. Zhang, J.J. Zhang, Chem. Soc. Rev. 41 (2012) 797.
[12] L.H. Bao, J.F. Zhang, X.D. Li, Nano Lett. 11 (2011) 1215.
[13] H.H. Xu, X.L. Hu, H.L. Yang, Y.M. Sun, C.C. Hu, Y.H. Huang, Adv. Energy Mater. 5 (2015) 201401882.
[14] L. Huang, D.C. Chen, Y. Ding, S. Feng, Z.L. Wang, M.L. Liu, Nano Lett. 13 (2013) 3135.
[15] X.H. Xia, Y.Q. Zhang, Z.X. Fan, D.L. Chao, Q.Q. Xiong, J.P. Tu, H. Zhang, H.J. Fan, Adv. Energy Mater. 5 (2015) 201401709.
[16] Y.X. Zeng, Y. Han, Y.T. Zhao, Y. Zeng, M.H. Yu, Y.J. Liu, H.L. Tang, Y.X. Tong, X.H. Lu, Adv. Energy Mater. 5 (2015) 201402176.
[17] J. Jiang, Y.Y. Li, J.P. Liu, X.T. Huang, C.Z. Yuan, X.W. (David) Lou, Adv. Mater. 24 (2012) 5166.
[18] L.Q. Mai, F. Yang, Y.L. Zhao, X. Xu, L. Xu, Y.Z. Luo, Nat. Commun. 2 (2011) 381.
[19] H.W. Lai, Q. Wu, J. Zhao, L.M. Shang, H. Li, R.C. Che, Z.Y. Lyu, J.F. Xiong, L.J. Yang, X.Z. Wang, Z. Hu, Energy Environ. Sci. (2016). http://dx.doi.org/10.1039/C6EE00603E.
[20] Y. Zhao, L.F. Hu, S.Y. Zhao, L.M. Wu, Adv. Funct. Mater. (2016). http://dx.doi.org/10.1002/adfm.201600494.
[21] S. Gao, Y. Sun, F. Lei, L. Liang, J. Liu, W. Bi, B. Pan, Y. Xie, Angew. Chem. Int. Ed. 53 (2014) 12789.
[22] Q. Liao, N. Li, S. Jin, G. Yang, C. Wang, ACS Nano 9 (2015) 5310.
[23] X. Jia, S. Cheng, L. Yang, Y. Jiang, Z. Jiang, C. Yang, H. Zhang, M. Liu, Nano Energy 11 (2015) 736.
[24] C. Zhu, P. Yang, D. Chao, W. Mai, H. Fan, Chem. Nano. Mater. 1 (2015) 458.
[25] C. Zhang, H. Yin, M. Han, Z. Dai, H. Pang, Y. Zheng, Y.Q. Lan, J. Bao, J. Zhu, ACS Nano 8 (2014) 761.
[26] M.H. Yu, W. Wang, C. Li, T. Zhai, X.H. Lu, Y.X. Tong, Npg. Asia Mater. 6 (2014) 129.
[27] X.L. Dong, Z.Y. Guo, Y.F. Song, M.Y. Hou, J.Q. Wang, Y.G. Wang, Y.Y. Xia, Adv. Funct. Mater. 24 (2014) 3405.
[28] W.P. Si, C.L. Yan, Y. Chen, S. Oswald, L.Y. Han, G.S. Oliver, Energy Environ. Sci. 6 (2013) 3218.
[29] M.F. El Kady, V. Strong, S. Dubin, R.B. Kaner, Science 335 (2012) 326.
[30] X.H. Lu, G.M. Wang, T. Zhai, M.H. Yu, S.L. Xie, Y.C. Ling, C.L. Liang, Y.X. Tong, Y. Li, Nano Lett. 12 (2012) 5376.

[31] X.H. Lu, M.H. Yu, T. Zhai, G.M. Wang, S.L. Xie, T.Y. Liu, C.L. Lian, Y.X. Tong, Y. Li, Nano Lett. 13 (2013) 2628.
[32] P.H. Yang, X. Xiao, Y.Z. Li, Y. Ding, P.F. Qiang, X.H. Tan, W.J. Mai, Z.Y. Lin, W.Z. Wu, T.Q. Li, H.Y. Jin, P.Y. Liu, J. Zhou, C.P. Wong, Z.L. Wang, ACS Nano 7 (2013) 2617.
[33] Z.L. Wang, Z. Zhu, J. Qiu, S. Yang, J. Mater. Chem. C 2 (2014) 1331.
[34] X.H. Lu, Y.X. Zeng, M.H. Yu, T. Zhai, C.L. Liang, S.L. Xie, M.S. Balogun, Y. Tong, Adv. Mater. 26 (2014) 3148.
[35] Y. Qian, R. Liu, Q. Wang, J. Xu, D. Chen, G. Shen, J. Mater. Chem. A 2 (2014) 10921.
[36] X. Wang, B. Liu, R. Liu, Q. Wang, X. Hou, D. Chen, R. Wang, G. Shen, Angew. Chem. Int. Ed. 126 (2014) 1880.
[37] X. Xiao, X. Peng, H. Jin, T. Li, C. Zhang, B. Gao, B. Hu, K. Huo, J. Zhou, Adv. Mater. 25 (2013) 5091.

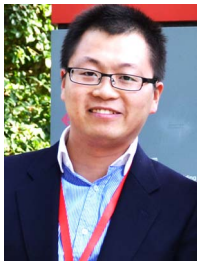

Huan Pang received his Ph.D. degree from Nanjing University in 2011. He then founded his research group in Anyang Normal University where he was appointed as a distinguished professor in 2013. Now, he also jointed Yangzhou University as a distinguished professor. His research interests include the development of inorganic semiconductors nanostructures and their applications in flexible electronics and printable electronics.

Wen-Yong Lai is a professor at Nanjing University of Posts and Telecommunications. He received his Ph.D from Fudan University in 2007. He then joined the Key Laboratory for Organic Electronics & Information Displays and Institute of Advanced Materials (IAM), Nanjing University of Posts & Telecommunications. His research mainly focuses on the design, synthesis, and application of organic & polymer optoelectronic materials for organic/plastic electronics. He is also interested in the exploration of novel materials and processes for printed/flexible electronics.

Zheng Hu received his BS (1985) and Ph.D. (1991) degrees in physics from Nanjing University. After two-year's postdoctoral research in Department of Chemistry, he became an associate professor in 1993, and subsequently acquired the professor position in 1999, and Cheung Kong Scholar professor in 2007. He is the owner of the highly competitive NSFC fund for outstanding young scientists of China (2005). As a guest scientist, he visited Research Center of Karlsruhe (Germany), University of Cambridge (UK), and MIT (USA) for two years. Hu is engaged in the research field of physical chemistry and materials chemistry addressing the growth mechanism, materials design and energy applications of a range of nano-/mesostructured materials, especially the carbon-based materials and group III nitrides.

Wei Huang received his PhD degree from Peking University in 1992. In 1993, he began his postdoctoral research in the Department of Chemistry under the supervision of Prof. Huang Hsing Hua in the National University of Singapore (NUS) and then taught at NUS. In the meantime, he took part in the foundation of the Institute of Materials and Engineering (IMRE), Singapore. In 2002, he moved to Fudan University where he founded the Institute of Advanced Materials (IAM). In 2006, he was appointed as the Deputy President of the Nanjing University of Posts and Telecommunications (NUPT). He was elected as an Academician of the Chinese Academy of Sciences in 2011. In 2012, he assumed his duty as the President of the Nanjing Tech University (NanjingTech). His research interests include organic/plastic/flexible (opto)electronics, nanomaterials and nanotechnology.